# Tree Hydrodynamic Modelling of Soil Plant Atmosphere Continuum (SPAC-3Hpy)

Marcela Silva[1], Ashley M. Matheny[2], Valentijn R.N Pauwels[1], Dimetre Triadis[3], Justine E. Missik[4], Gil Bohrer[4], and Edoardo Daly[1]

[1]Department of Civil Engineering, Monash University, Clayton, VIC, Australia

[2]Department of Geological Sciences, Jackson School of Geosciences, University of Texas at Austin, TX, USA

[3]Department of Mathematics and Statistics, La Trobe University, Bundoora, VIC, Australia

[4]Department of Civil, Environmental and Geodetic Engineering, Ohio State University, OH, USA

**Correspondence:** Marcela Silva (marcela.defreitassilva@monash.edu), Edoardo Daly (edoardo.daly@monash.edu)

**Abstract.** Modelling the water transport along the soil-plant-atmosphere continuum is fundamental to estimating and predicting transpiration fluxes. A tree-hydrodynamic model (SPAC-3Hpy) for the water fluxes across the soil-plant-atmosphere continuum is presented here. The model combines the water transport pathways to one vertical dimension, and assumes that the water flow through the soil, roots, and above-ground xylem can be approximated as a flow in porous media. This results in a system of three

5  partial differential equations resembling the Richardson-Richards equation describing the transport of water through the plant system and with additional terms representing sinks and sources for the transfer of water from to the soil to the roots and from the leaves to the atmosphere. The numerical scheme, developed in Python 3, was tested against exact analytical solutions for steady state and transient conditions using simplified but realistic model parametrizations. The model was also used to simulate a previously published case study where observed transpiration rates were available in order to evaluate model performance.

10  With the same model setup as the published case study, SPAC-3Hpy results were in agreement with observations. Through a rigorous coupling of soil, roots, and hydroactive xylem, SPAC-3Hpy can account for variable capacitance while conserving mass and the continuity of the water potential between these three layers. SPAC-3Hpy provides a ready-to-use open access numerical model for the simulation of water fluxes across the soil-plant-atmosphere continuum.

# 1 Introduction

Plant transpiration drives the exchange of water and energy between the land and atmosphere (Katul et al., 2012), influencing ecosystem carbon uptake, as well as the partitioning of rainfall into evapotranspiration, runoff, and groundwater recharge. Transpiration fluxes are driven by complex biological and physical processes, which, by interacting with each other, link the soil to the atmosphere through the above- and below-ground structures of plants. Several approaches exist to model the transpiration fluxes from the soil to the atmosphere (Fatichi et al., 2016; Matheny et al., 2017; Mencuccini et al., 2019).

Most models that explicitly resolve the movement of water within the plant system rely on the cohesion-tension theory, which explains how water can be transferred upward from the soil to the atmosphere across a tree height of several meters. An uninterrupted water column can extend from the roots to the leaves under tension and, as the stomata open, water is transferred to the atmosphere pulling water from the soil, through the roots and xylem (Steudle, 2001). Accordingly, the system composed by the Soil, Plant, and Atmosphere is interpreted as a Continuum (SPAC) with water flowing through its different compartments following a path of decreasing water potentials (Nobel, 2009).

In this context, the first models proposed to describe transpiration fluxes used an electrical analogy, with water flowing from one compartment to the other following water potential gradients associated across plant conductive tissue with resistances to the flow (van den Honert, 1948; Cowan, 1965; Jones, 2009). Recent advances in these models account for the water storage within the plant using capacitors, and link the water and $CO_2$ fluxes through the stomatal conductance (Cruiziat et al., 2002; Daly et al., 2004b, a; Manzoni et al., 2013; Bartlett et al., 2014; Manoli et al., 2014; Hartzell et al., 2018). Such electrical-circuit equivalence models commonly assume that the water flow along the SPAC occurs as a succession of steady states, whereby the water potentials in the different compartments of the system adjust instantaneously to environmental changes.

This assumption of steady state is relaxed in models that describe the water flow in the soil and plant xylem as flow in porous media (Fruh and Kurth, 1999). Porous-media models combine the continuity equation with the Darcy's law to define partial differential equations for the dynamics of the water potential across the SPAC. Some applications of these models focus on the water fluxes within the plant architecture (Kumagai, 2001; Bohrer et al., 2005; Chuang et al., 2006; Janott et al., 2011), others are centred on processes below-ground and the interaction between soil and roots (Somma et al., 1998; Mendel et al., 2002; Amenu and Kumar, 2007; Teodosio et al., 2017), with more recent applications looking at the whole SPAC system (Verma et al., 2014; Quijano and Kumar, 2015; Mirfenderesgi et al., 2016, 2018). Although more complex than electrical circuit models, porous-media models are able to simulate a larger variety of processes, such as root water compensation and hydraulic redistribution (Verma et al., 2014), and account for the transient response of water potential along the SPAC system. Porous-media models that simulate the entire tree structure, with a detailed 3D representation of branches and root systems, are computationally demanding and require specific and complex parameterizations. As a result, application of these models is impracticable to simulate water flow in more than a single tree (Bohrer et al., 2005; Janott et al., 2011). One-dimensional models that lump within-tree spatial hydraulic variability in their parameters are a more practical option to represent water movement in individual trees and within stands (Amenu and Kumar, 2007; Quijano and Kumar, 2015; Mirfenderesgi et al., 2016, 2018).

The aim of this study is to present the Soil-Plant-Atmosphere Continuum Tree Hydrodynamic model (SPAC-3Hpy), an open
50  access tree hydrodynamic model for the simulation of the temporal and vertical dynamics of water storage and fluxes from
the soil to the atmosphere, accounting for the vegetation response to environmental conditions and soil water availability. As a
porous-media model, SPAC-3Hpy solves a system of three partial differential equations in a 1D domain to describe the water
flow through the soil, root, and stem xylem. The primary novelty of the model is a full coupling of the soil, roots, and xylem by
clarifying the links between these 3 components of the system when lumping the processes into a single, continuous vertical
55  dimension. The numerical formulation of SPAC-3Hpy was verified against exact solutions of simplified expressions of the
equations, and the model performance was evaluated against observational data collected during six months from a case study.

## 2  Model description

### 2.1  Model overview

SPAC-3Hpy builds upon FETCH2 (Mirfenderesgi et al., 2016, 2018), which is based on its precursor, the finite element tree
60  crown hydrodynamics (FETCH) model (Bohrer et al., 2005). FETCH simulates water flow along a tree's stem and branches
accounting for the branch structure in three dimensions, while FETCH2 simplifies branches along the vertical direction leading
to a 1D model (Mirfenderesgi et al., 2016).

Similarly to FETCH and FETCH2, SPAC-3Hpy assumes that the water movement in the xylem resembles flow in porous
media, and uses a macroscopic approach, lumping soil, roots, and stems along the vertical direction (Fig. 1). In SPAC-3Hpy,
65  water in a variably saturated soil is exchanged between the soil and the root system. The water flow in the soil is modelled
using the Richardson-Richards equation with a term simulating the exchange of water between the soil and the roots. This term
is a function of the difference in water potential between the soil and root layers; it thus results in water sink during the day,
when the water potential in the roots is low due to water loss by transpiration, but may act as source of water to the soil during
the night when the roots are near saturation, depending on the water content in different soil layers.

70  Water fluxes within roots are likewise modelled with a Richardson-Richards type equation with the same term (of the opposite
sign) representing water exchange between roots and soil. Soil and roots are coupled through this term, such that a sink of water
in the soil is a source of water in the roots, and vice versa. The 3D root architecture is lumped along the vertical dimension
using a vertical mass distribution of the roots and an index that summarizes the extent of lateral root area per unit of ground
area (Quijano and Kumar, 2015). Water fluxes through the soil are defined as the mass flow of water per unit of ground volume.
75  Thus, when referring the water fluxes in the roots to the same water mass that was contributed by the soil, the water storage and
water fluxes within the roots must be re-scaled to the ground volume and thus, when normalized by unit depth, to the ground
area.

A similar approach is used to model the water flow in the above-ground xylem, which is also described with a Richardson-
Richards type equation with a sink term associated with transpiration losses from the canopy to the air. This equation is
80  commonly used to simulate water flow for a single tree (Chuang et al., 2006); however, in order to correctly couple the above-
ground and the below-ground components of the system, both equations must refer the water flux to units of ground area.

This ensures the water mass balance and the continuity of the fluxes from soil through the root system to the above-ground xylem and ultimately to the air. This conservation of flux throughout the system is important but not trivial, as the amount of roots that fits within a reference area of soil, for example, is different than the xylem area or leaf area which are located

85  above the same area of soil. SPAC-3Hpy simulates variable plant water storage below- and above-ground by using a dynamic capacitance function. Accounting for whole-plant water storage enables different model applications in which plant storage plays an important role, such as water use efficiency and plant hydraulic stress during drought periods (Huang et al., 2017; Li et al., 2021).

The complete system of equations simulates the water fluxes assuming a spatial distribution of tree, and their associate roots,

90  stem xylem, and leaves, with an average cross-sectional area per unit of ground area. In this manner, SPAC-3Hpy presents a novel up-scaling technique required to properly calculate tree transpiration from small and large areas, such as a forest stand or plantations, assuming that all trees within the simulated area are similar on their dimensions and conductive parameters.
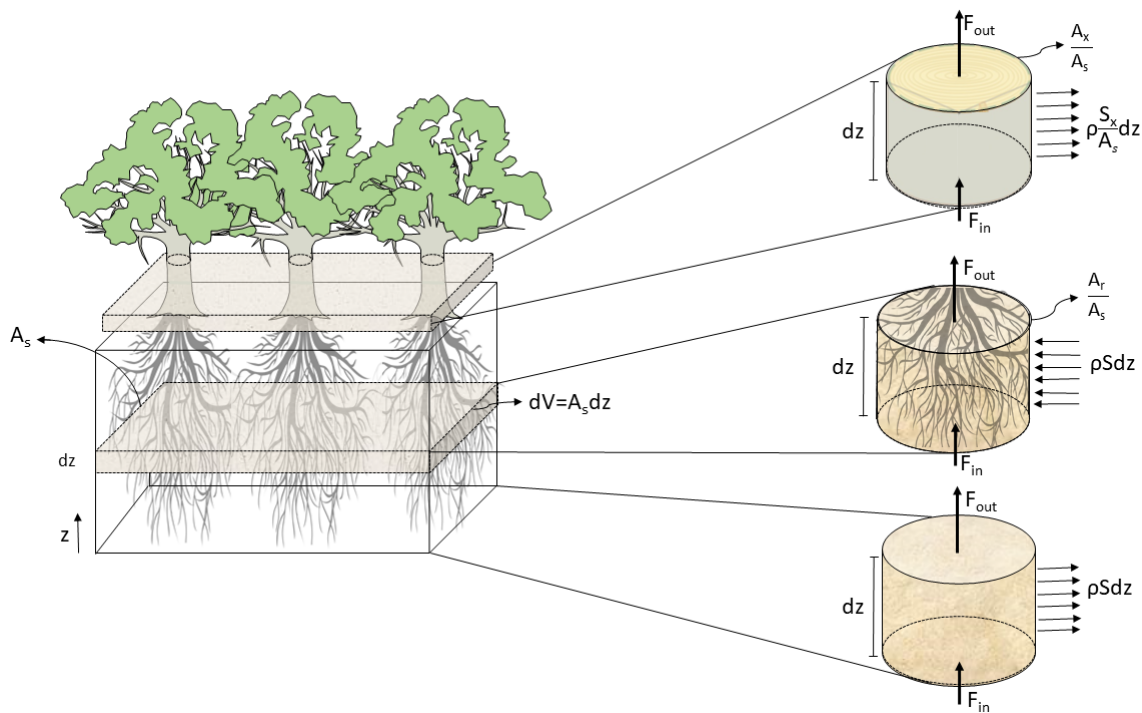


**Figure 1.** Representation of the coupling process between soil, roots, and stem xylem applied in the model

## 2.2 Governing equations

A detailed derivation of the equations is provided in the supplementary material and only the final set of equations is reported

95  here for brevity.

Water flow in a variably saturated soil is described using the Richardson-Richards equation with a sink term for root water uptake:

$$C_s \frac{\partial \Phi_s}{\partial t} = \frac{d\theta_s}{d\Phi_s} \frac{\partial \Phi_s}{\partial t} = \frac{\partial}{\partial z}\left[ K_s \left( \frac{\partial \Phi_s}{\partial z} + \rho g \right)\right] - S, \tag{1}$$

where $C_s$ (Pa$^{-1}$) is the soil capacitance, $\Phi_s$ (Pa) is the soil water potential, $\theta_s$ (m$^3$ m$^{-3}$) is the soil volumetric water content, $K_s$ (m$^2$ s$^{-1}$ Pa$^{-1}$) is the effective soil hydraulic conductivity, $\rho$ (kg m$^{-3}$) is the water density, $g$ (m s$^{-2}$) is the gravitational acceleration, $S$ ($s^{-1}$) is the root water uptake, and $t$ (s) is time, and $z$ (m) is distance along vertical direction, assuming positive represents upward flux. The relationships between $K_s$, $\Phi_s$ and $\theta_s$ are modelled according to van Genuchten (1980).

Considering the cross-sectional area of roots ($A_r$) per unit of ground area ($A_s$), the equation describing the water flow through the roots reads

$$C_r \frac{\partial \Phi_r}{\partial t} = \frac{d}{d\Phi_r}\left( \frac{\theta_r A_r}{A_s} \right) \frac{\partial \Phi_r}{\partial t} = \frac{\partial}{\partial z}\left[ K_r \frac{A_r}{A_s} \left( \frac{\partial \Phi_r}{\partial z} + \rho g \right)\right] + S, \tag{2}$$

where $C_r$ (Pa$^{-1}$) is the root capacitance, $\Phi_r$ (Pa) is the root water potential, $\theta_r$ is the root volumetric water content, $K_r$ (m$^2$ s$^{-1}$ Pa$^{-1}$) is the effective axial hydraulic conductivity of the roots, and $A_r/A_s$ (m$^2_{root}$ m$^{-2}_{ground}$) is the root cross sectional area index, representing the total root cross-sectional area at a given elevation per unit of ground area.

Above-ground, the flow through the cross-sectional area of hydroactive stem xylem ($A_x$) per unit ground area is given by

$$C_x \frac{\partial \Phi_x}{\partial t} = \frac{d}{d\Phi_x}\left( \frac{\theta_x A_x}{A_s} \right) \frac{\partial \Phi_x}{\partial t} = \frac{\partial}{\partial z}\left[ K_x \frac{A_x}{A_s} \left( \frac{\partial \Phi_x}{\partial z} + \rho g \right)\right] - \frac{S_x}{A_s}, \tag{3}$$

where $C_x$ (Pa$^{-1}$) is the stem xylem capacitance, $\Phi_x$ (Pa) is the stem xylem water potential, $\theta_x$ (m$^3$ m$^{-3}$) is the stem xylem volumetric water content, $K_x$ (m$^2$ s$^{-1}$ Pa$^{-1}$) is the effective axial hydraulic conductivity of the stem, $S_x$ ($m^2 \ s^{-1}$) is the flow of water leaving the xylem per unit of length due to transpiration, and $A_x/A_s$ (m$^2_{stem}$ m$^{-2}_{ground}$) is a hydroactive stem-xylem cross-sectional area index. This index can be calculated from the tree sapwood area and stand density (typically reported for forest plots as number of trees per hectare), representing the total sapwood area per unit of ground area. The cross sectional area indicies applied to the roots and stem guarantee the conservation of water as it flows across soil, roots, and stem.

### 2.2.1 Root water uptake and transpiration

Eqs. (1) and (2) are coupled through the exchange of water between the soil and roots. The term $S$ is modelled as a function of the difference between the water potential in the soil and the roots. This approach, introduced by Gardner (1960), was applied in several studies (Herkelrath et al., 1977; Mendel et al., 2002; Amenu and Kumar, 2007). Accordingly, $S$ (s$^{-1}$) is expressed as

$$S(z,t) = k_{s,rad} \ f(\theta_s) \cdot A_{ind}(z) \cdot \frac{r(z)}{\int_{z_{r_i}}^{z_{r_j}} r(z)dz} \cdot (\Phi_s - \Phi_r), \tag{4}$$

where $k_{s,rad}$ (m$^3$s$^{-1}$m$_{root}^{-2}$Pa$^{-1}$) is the soil-to-root radial conductance per unit of root surface area, $f(\theta_s)$ is a dimensionless reduction function due to soil moisture, $A_{ind}$ (m$^2_{\text{root}}$m$^{-2}_{\text{ground}}$) is an index defining the lateral root surface area per ground area,

125 and $r(z)$ the root mass distribution, with $z_{r_i}$ and $z_{r_j}$ (m) representing the elevation of the bottom and top of the roots.

The water lost to the atmosphere is calculated using a transpiration function that limits the amount of water leaving the stomata as a function of the stem water potential. Accordingly, $S_x/A_s$ (s$^{-1}$) reads

$$\frac{S_x}{A_s} = T \cdot l(z), \tag{5}$$

where $T$ (m s$^{-1}$) is the transpiration rate, which is distributed along the canopy height via the leaf area density distribution

130 ($l(z)$, m$^2$ m$^{-2}$ m$^{-1}$), which is the leaf area per unit of ground area per unit of height, which integrates vertically to the leaf area index (LAI). This effectively assumes that transpiration is proportional to leaf area throughout the depth of the canopy. We have found that in canopies where most leaves are concentrated near the upper layers, the results are not very sensitive to this simplification. More complex representations of the vertical distribution of transpiration through the canopy depth have been developed. Such vertically detailed canopy transpiration models assume, for example, that transpiration is vertically distributed

135 proportionally to vertical light extinction through the depth of the canopy (Shaw and Schumann, 1992; Bohrer et al., 2009), or that transpiration rate is vertically distributed as a function that combines light attenuation and the vertical profiles of other physical radiative forcing, such as turbulence, wind speed, temperature, and humidity (Bonan et al., 2018; Drewry et al., 2010). Such transpiration models can be easily implemented in SPAC-3Hpy, simply by replacing Eq. (5) with a more elaborate vertical redistribution scheme, provided that the vertical descriptions of the required parameters for leaf area density, light attenuation

140 and other physical forcing are available for the simulated forest plot.

## 2.3 Numerical scheme

Eqs. (1) - (3) are solved simultaneously using a finite difference numerical scheme, following Celia et al. (1990). The equations are solved using a fully implicit Picard method, with a backward Euler temporal discretization, as detailed in the Supplementary Material. The scheme is implemented in Python 3 in modular manner (i.e., with subroutines to define effective conductances

145 and the capacitance of the soil, roots, and stem).

## 3 Model experiments

Three applications were used to i) test the correctness of the numerical scheme against analytical solutions, ii) compare results to a published case study, and iii) show the implementation of a leaf area density profile.

## 3.1 Testing against analytical solutions

150 The numerical scheme was tested against three simplified cases that permit the derivation of solutions in closed form. Because of the nonlinear nature of the Richardson-Richards equation, only a few exact solutions are available, particularly when including sink and source terms (Broadbridge et al., 2017). An exact solution of the combined soil-to-air system (Eqs. 1 - 3) is thus

too challenging to be derived. Therefore, the numerical scheme was tested against one of the equations. Eq. (3) was selected
for this exercise and it was re-written as

$$\frac{\partial}{\partial t}\left(A_x\,\theta_x\right) = \frac{\partial}{\partial z}\left(A_x\,K_x\frac{\partial \Phi_x}{\partial z}\right) + \frac{\partial}{\partial z}\left(A_x\,K_x\rho g\right) - S_x, \tag{6}$$

where $S_x = lA_xT$, and $T = T(\Phi_x, z, t)$ (m s$^{-1}$) is the transpiration rate; $z$ (m) is bound between 0 at the bottom of the tree
and $L$ at the top of the tree.

For analytical tractability of Eq. (6), simplified formulations of the hydraulic conductivity and capacitance are used. The
hydraulic conductivity is assumed to decrease with the water potential following the vulnerability curve (Bohrer et al., 2005;
Chuang et al., 2006)

$$K_x = K_m\,e^{\alpha_0 \Phi_x}, \tag{7}$$

with $\alpha_0$ (Pa$^{-1}$) an empirical constant and $K_m$ (m$^2$ s$^{-1}$ Pa$^{-1}$) the maximum hydraulic conductivity. Eq. (7) implies that
$d\Phi_x = dK_x/(\alpha_0 K_x)$. The xylem water content is assumed to depend on $\Phi$ according to

$$\theta_x = \theta_{res,x} + (\theta_{sat,x} - \theta_{res,x})\,e^{\alpha_0 \Phi_x}, \tag{8}$$

with $\theta_{res,x}$ (-) and $\theta_{sat,x}$ (-) being the residual and maximum water content of the stem xylem.

With the further assumption that $A_x = A_0\exp(-\beta z)$, with $\beta$ (m$^{-1}$) an empirical allometric parameter, Eq. (6) can be re-written
as

$$\gamma_0\frac{\partial K_x}{\partial t} = \frac{1}{\alpha_0}\frac{\partial^2 K_x}{\partial z^2} + \left(\rho g - \frac{\beta}{\alpha_0}\right)\frac{\partial K_x}{\partial z} - \rho g\beta K_x - lTe^{\beta z}, \tag{9}$$

where $\gamma_0 = (\theta_{sat,x} - \theta_{res,x})/K_m$, (s Pa m$^{-2}$).

Assuming that at time $t = 0$ the water head is $\Phi_x(z, 0)$, the initial condition for Eq. (9) reads

$$K_x(z, 0) = K_m e^{\alpha_0 \Phi_x(z, 0)}. \tag{10}$$

The boundary condition at the bottom of the tree is defined by a time series of water potential (i.e., $\Phi_0 = \Phi_x(0, t)$), which
results in

$$K_x(0, t) = K_m e^{\alpha_0 \Phi_0(t)}. \tag{11}$$

The flux of water at the top of the tree ($z = L$) is zero, leading to the boundary condition

$$\left(\frac{1}{\alpha_0}\frac{\partial K_x}{\partial z} + K_x\rho g\right)_{z=L} = 0. \tag{12}$$

Solutions of Eq. (9) with initial and boundary conditions in Eqs. (10) - (12) can be obtained for different expressions of $T(z, t)$
for some cases as presented in the following sections.

### 3.1.1 Simplified unsteady case

180 An exact solution of Eq. (9) can be obtained by assuming $\beta = 0$ and considering that the gradient of water potentials is the main contributor to the water fluxes (i.e., neglecting the term $\partial_z(A_x \, K_x \rho g)$ in Eq. 6). With these assumptions, Eq. (9) becomes a linear diffusion equation with a sink term that can be re-written in compact form as $f_x(z,t) = lT$ and the boundary condition at the top of the tree reading $(\partial_z K_x/\alpha_0)_{z=L} = 0$.

A general solution of this equation can be written as (Polyanin, 2001)

$$185 \quad K_x(z,t) = \int_0^L K_x(\xi,t)G(z,\xi,t)d\xi + \frac{1}{\gamma_0\alpha_0}\int_0^t K_x(0,\tau)\left[\frac{\partial}{\partial \xi}G(x,\xi,t-\tau)\right]_{\xi=0}d\tau + \int_0^t\int_0^L f_x(\xi,\tau)G(z,\xi,t-\tau)d\xi d\tau, \quad (13)$$

where

$$G(x,\xi,t) = \frac{2}{L}\sum_{n=0}^{\infty}\sin\left[\frac{\pi(2n+1)x}{2L}\right]\sin\left[\frac{\pi(2n+1)\xi}{2L}\right]\exp\left[-\frac{\pi^2(2n+1)^2t}{4L^2\gamma_0\alpha_0}\right]. \quad (14)$$

For a case where transpiration depends only on time, the sink is expressed as

$$f_x = T_m(1-\cos(2\pi t/24)), \quad (15)$$

190 where $T_m$ is the maximum transpiration rate, $t$ is considered to be in hours, and it is assumed that $l = 1 \, (\mathrm{m}^{-1})$.

A fixed potential, equal to 0 MPa, was considered at the bottom of the stem and along the vertical direction as initial condition. This solution was tested for a 6 m high tree with the parameters listed in Table 1. Comparisons between the exact and numerical solutions using the sink term in Eq. (15) are shown in Fig (2). The errors associated with the numerical solution are small, reaching a maximum of approximately $0.25 \cdot 10^{-3}$ MPa at the top of the tree. The error followed the pattern of transpiration,

195 reaching its peak during day time and corresponding to a maximum error of 0.09% of the exact solution. Similarly, the lowest error could be observed at night, when transpiration approaches zero. The numerical solution presents errors that change periodically. After the influence of the initial condition disappears, the errors remain stable in time.

For a case where transpiration depends on both time ($t$) and the vertical position ($z$), the sink is written as

$$f_x = T_m \, z \, (1-\cos(2\pi t/24)), \quad (16)$$

200 where $l = z \, (\mathrm{m}^{-1})$.

Comparisons between the analytical and numerical solutions using Eq. (16) are shown in Fig. 3, where 0 MPa was assumed at the bottom of the tree and as initial condition along the vertical direction. The error for this case is higher than for the previous case, with a maximum value that is about 0.2% of the exact solution. These errors would reduce using smaller values of $\Delta z$.

### 3.1.2 Steady-state solution

205 A solution of Eq. (9) at steady state can be obtained accounting for effects due to gravity and using a distribution of leaf area per unit of stem height. It is assumed that the leaf area per unit of height is compatible with the Eq. (13) and satisfies $l(0) = 0$,
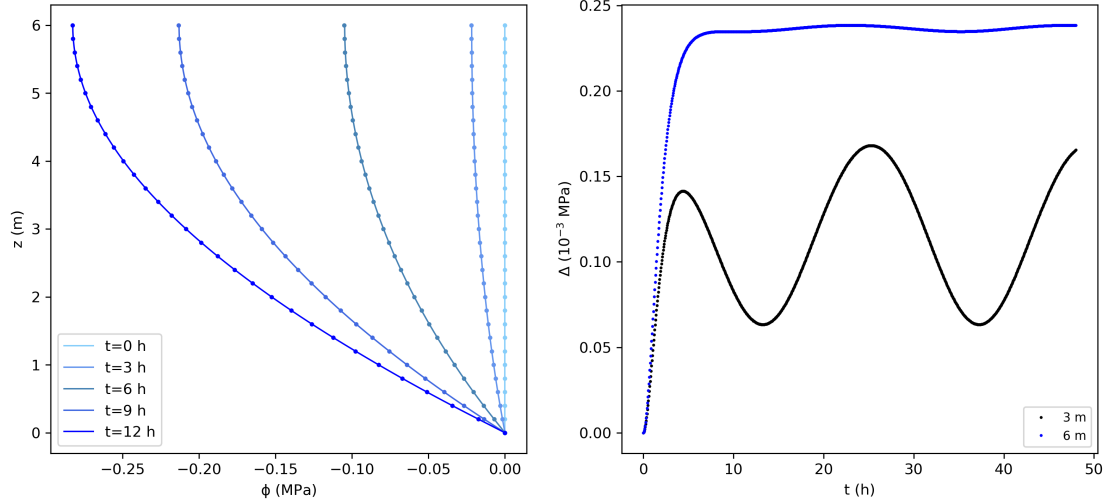
**Figure 2.** Left: water potentials (MPa) from the exact (lines) and numerical solutions (dots) using the sink term in Eq. (15) for the first 12 hours. For better visualization not all points are shown for the numerical solution. Right: difference between the exact and numerical solution ($\Delta$) at 3 m and 6 m. The temporal and spatial resolutions are 0.05 h and 0.01 m, respectively.
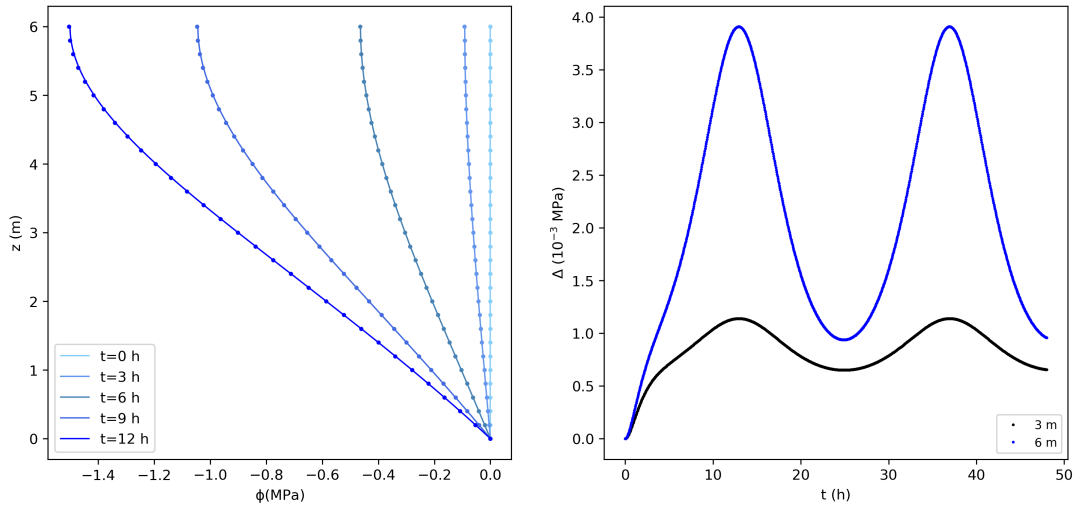


**Figure 3.** Left: water potentials (MPa) from the exact (lines) and numerical solutions (dots) using the sink term in Eq. (16) for the first 12 hours. For better visualization not all points are shown for the numerical solution. Right: difference between the exact and numerical solution ($\Delta$) at 3 m and 6 m. The temporal and spatial resolutions are 0.05 h and 0.01 m, respectively.

a possible expression for l(z) is

$$l(z) = \frac{l_m \beta_1}{\beta_2 - \beta_1} \left( \frac{\beta_2}{\beta_1} \right)^{\frac{\beta_2}{(\beta_2 - \beta_1)}} \left( e^{-\beta_1 z} - e^{-\beta_2 z} \right), \tag{17}$$

with $\beta_2 > \beta_1$. It is also assumed that the transpiration rate depends on the water potential and the elevation as

$$T = T_m e^{\alpha_0 \Phi_x} e^{\beta_1 - \beta}. \tag{18}$$

Accordingly, Eq. (9) at steady state reads

$$\frac{1}{\alpha_0} \frac{\partial^2 K_x}{\partial z^2} + \left( \rho g - \frac{\beta}{\alpha_0} \right) \frac{\partial K_x}{\partial z} - \rho g \beta K_x + \zeta(e^{-\eta-1})K_x = 0, \tag{19}$$

where $\eta = \beta_2 - \beta_1 > 0$ and

$$\zeta = \frac{l_m T_m \beta_1}{A_0 K_m (\beta_2 - \beta_1)} \left( \frac{\beta_2}{\beta_1} \right)^{\beta_2/(\beta_2 - \beta_1)}. \tag{20}$$

If it is assumed that the water potential initially has a generic profile and at the bottom of the tree remains constant in time, the water potential will stabilize in time to a steady profile with the flux of water from the bottom of the tree equalling the flux of water being lost via transpiration.

The solution of Eq.(19) can thus be written as

$$K(z) = C_1 y^{(\alpha_0 - \beta)/\eta} J_\upsilon(y) + C_2 \, y^{(\alpha_0 - \beta)/\eta} Y_\upsilon(y), \tag{21}$$

where $J_\upsilon$ (.) and $Y_\upsilon$ (.) are the Bessel functions of the first and second kind (Abramowitz and Stegun, 1964) of order

$$\upsilon = \frac{[4\alpha_0 \zeta + (\alpha_0 + \beta)^2]^{1/2}}{\eta}, \tag{22}$$

and $C_1$ and $C_2$ are constants to be determined numerically by imposing the boundary conditions, as in Eqs. (11) and (12) with $\Phi_0$ constant.

The agreement between the exact and numerical solutions is shown in Fig. (4), for a case considering a bottom boundary condition of $\Phi_0=0$ MPa, a no-flux boundary condition at the top, and a hydrostatic initial condition. Steady state was reached after a short interval of about 3 hours of model time set. For a 6 meter high tree, the error of the numerical solution increases with elevation reaching approximately $0.4 \cdot 10^{-3}$ MPa at the tree top, being 0.4% of the exact value. A larger error was reached in comparison to the unsteady state solution cases due to the more complex formulation used for the steady-case scenario.

### 3.2 Model application

SPAC-3Hpy was tested against a case study described in Verma et al. (2014). For reproducibility purposes, SPAC-3Hpy used the same model setup, environmental variables, and parameters as Verma et al. (2014), where the software COMSOL Multiphysics (Ver. 4.1; http://www.comsol.com/) was selected to solve the system of equations using finite elements. Details of the dataset are reported in Zeppel et al. (2008), Yunusa et al. (2012), and Verma et al. (2014), with a brief summary presented here.

### 3.2.1 Site description

The study site is located at latitude 33°39' 41" S and longitude 150°46' 57" E in New South Wales, Australia. According to the long term statistics (1993–2013 - Royal Australian Air Force base in Richmond, Australian Bureau of Meteorology, station
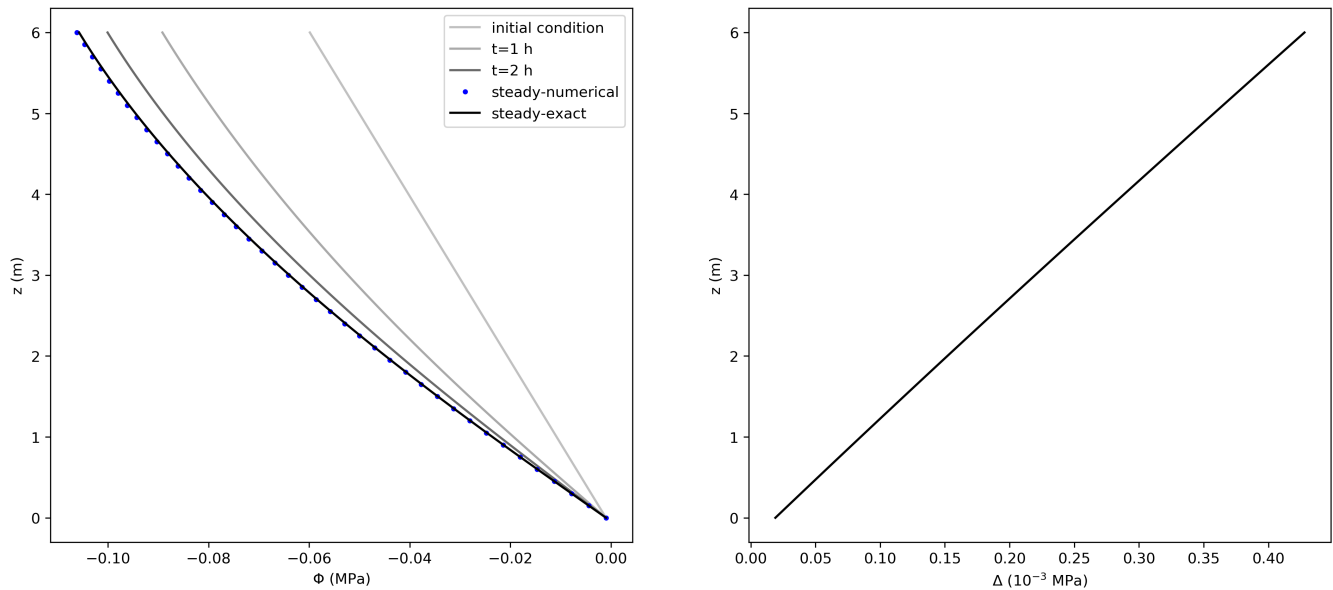
**Figure 4.** Left: water potentials, $\Phi$, (MPa) at steady state obtained from the exact (black line) (Eq. 21), and numerical solutions (dots), using 0.05 m and 0.08 h as spatial and temporal resolution, respectively. For the numerical solution, not all points are shown for better visualization. The line with light colors present the initial condition and the first 2 hours of simulation. Right: difference between the exact and numerical solution ($\Delta$) at steady state condition along tree height.

**Table 1.** List of parameters used in the comparison between the exact and numerical solutions (section 3.1)

| Parameters | Value | Units | Description |
|---|---|---|---|
| $\beta$ | 0 | $\mathrm{m}^{-1}$ | Allometric parameter, vertical reduction rate of cross-sectional area |
| $\beta_1$ | 0.2 | $\mathrm{m}^{-1}$ | Empirical shape parameter for vertical leaf area distribution per unit xylem lenght |
| $\beta_2$ | 1 | $\mathrm{m}^{-1}$ | Empirical shape parameter for vertical leaf area distribution per unit xylem lenght |
| $l_m$ | 0.2 | m | Mean leaf area per unit of length |
| $A_0$ | 0.0045 | $\mathrm{m}^2$ | Basal cross-sectional area of the stem xylem |
| $T_m$ | $3.47 \cdot 10^{-8}$ | $\mathrm{m\,s}^{-1}$ | Maximum transpiration rate |
| $\alpha_0$ | $5 \cdot 10^{-7}$ | $\mathrm{Pa}^{-1}$ | Empirical constant |
| $\theta_{res,x}$ | 0.1 | - | Residual water content of the stem xylem |
| $\theta_{sat,x}$ | 0.6 | - | Saturated water content of the stem xylem |
| $K_m$ | $1.02 \cdot 10^{-9}$ | $\mathrm{m^2\,s^{-1}Pa^{-1}}$ | Maximum hydraulic conductivity |

067105, http://www.bom.gov.au/climate/data/) the average daily minimum and maximum temperatures are 10 °C and 24 °C, with annual rainfall approximately 730 mm.

Geoscientific
Model Development
Discussions

Rainfall, solar radiation, air temperature, and humidity were collected every 30 minutes from January 1st to June 4th in 2007.

240 Sap flux data were collected for the same period, using the heat ratio technique at a half-hour resolution. The vegetation is dominated by *Eucalyptus parramattensis* C.A. Hall (Parramatta red gum) and *Angophora bakeri* E.C. Hall (narrow-leaved apple). The trees were 14 m tall on average, with a LAI between 1.3 and 1.9.

The soil is duplex, with a first layer up to a depth of 0.8 m being predominantly sand , with clay underneath. The soil parameters used in the model are listed in Table 2.

**Table 2.** List of soil parameters used in the model application

| Parameters | Units | Sand | Clay | Description |
|---|---|---|---|---|
| $k_{s,sat}$ | m s$^{-1}$ | $3.45 \cdot 10^{-5}$ | $1.94 \cdot 10^{-7}$ | Saturated hydraulic conductivity |
| $\theta_{sat}$ | – | 0.47 | 0.55 | Saturated volumetric soil moisture content |
| $\theta_{res}$ | – | 0.045 | 0.068 | Residual volumetric soil water content |
| $\alpha$[1] | m$^{-1}$ | 14.5 | 0.8 | van Genuchten parameter |
| $n$[1] | – | 2.4 | 1.5 | van Genuchten parameter |
| $\theta_1$[1] | – | 0.05 | 0.08 | Root water uptake reduction function parameter |
| $\theta_2$[1] | – | 0.09 | 0.12 | Root water uptake reduction function parameter |

[1] Definitions and equations using these parameters can be found in the Supplementary Material.

## 245 3.2.2 Model setup

The system of equations was solved for a soil depth of 5 m, and trees with a height of 14 m and root depth of 3.2 m. The boundary condition at the soil bottom was a constant water potential equal to -0.06 MPa, corresponding to a water content of $0.28 \, \mathrm{m^3 m^{-3}}$. At the surface, measured rainfall was used as a flux boundary condition. The boundary conditions for the trees are a zero-flux condition at the bottom of the roots and, above-ground, transpiration is applied as a boundary condition at the top

250 of the canopy. Daytime transpiration is modelled through the Penman Monteith equation (Allen et al., 1998) combined with a stomata conductance function (Jarvis, 1976), whereas night time transpiration follows a more simplified formulation composed of a constant nightime transpiration value modulated by temperature, VPD, and water potential at night (See Supplementary Material for more details). In order to follow the same setup as in Verma et al. (2014), transpiration is not distributed along the stem, but is imposed as a flux concentrated at the top of the tree. For the same reason, the capacitance of the xylem in the roots

255 and stem is assumed constant (Verma et al., 2014).

In the sand layer, soil initial conditions are assumed to be a constant water potential equal to -0.004 MPa, corresponding to a water content of $0.08 \, \mathrm{m^3 m^{-3}}$. In the clay layer, water potential below a depth of 3 m was constant and equal to -0.06 MPa. Between these two depths, water potential was interpolated linearly. For the tree, water potential linearly decreased from -0.06 MPa at the bottom of the roots to -0.22 MPa at the top of the canopy. The spatial resolution used was 0.1 m, and the time step

260 20 s. The list of parameters used in the model, including root water uptake and transpiration parameters, is in Table 3.

**Table 3.** List of parameters used in the application of the model as in Verma et al. (2014)

| Parameters | Units | Value | Description |
|---|---|---|---|
| $A_x/A_s$ | - | $8.6 \cdot 10^{-4}$ | Stem xylem cross sectional area index surface ratio |
| $A_r/A_s$ | - | 1 | Root xylem cross sectional area index |
| $A_{ind}$ | - | 1 | Lateral root surface area index |
| LAI | - | 1.5 | Leaf area index |
| $k_{s,rad}$ | $\text{s}^{-1}$ | $7.2 \cdot 10^{-10}$ | Total soil-to-root radial conductance |
| $C_x$ | $\text{Pa}^{-1}$ | $1.1 \cdot 10^{-11}$ | Stem xylem capacitance |
| $C_r$ | $\text{Pa}^{-1}$ | 1 | Root xylem capacitance |
| $h$ | m | 14 | Tree height |
| $C_p$ [1] | $\text{J m}^{-3}\,\text{K}^{-1}$ | 1200 | Heat capacity of air |
| $T_{opt}$ [1] | K | 289.15 | Jarvis temperature parameter |
| $\lambda$ [1] | $\text{J m}^{-3}$ | $2.51 \cdot 10^9$ | Latent heat of vaporization |
| $\gamma$ [1] | $\text{Pa K}^{-1}$ | 66.7 | Psychometric constant |
| $g_b$ [1] | $\text{m s}^{-1}$ | $2 \cdot 10^{-2}$ | Leaf boundary layer conductance |
| $g_a$ [1] | $\text{m s}^{-1}$ | $2 \cdot 10^{-2}$ | Aerodynamic conductance |
| $k_r$ [1] | $\text{m}^2\,\text{W}^{-1}$ | $5 \cdot 10^{-3}$ | Jarvis radiation parameter |
| $k_t$ [1] | $\text{K}^{-2}$ | $1.6 \cdot 10^{-3}$ | Jarvis temperature parameter |
| $k_d$ [1] | $\text{Pa}^{-1}$ | $1.1 \cdot 10^{-3}$ | Jarvis vapor pressure deficit parameter |
| $h_{x50}$ [1] | m | -130 | Jarvis leaf water potential parameter |
| $g_{smax}$ [1] | $\text{m s}^{-1}$ | $10 \cdot 10^{-3}$ | Maximum leaf stomatal conductance |
| $n_l$ [1] | - | 2 | Jarvis leaf water potential parameter |
| $E_{max}$ [1] | $\text{m s}^{-1}$ | $1 \cdot 10^{-9}$ | Maximum night time transpiration |
| $q_z$ [1] | - | 9 | Root distribution parameter |
| $k_{max}$ [1] | $\text{m s}^{-1}$ | $1 \cdot 10^{-5}$ | Maximum conductivity of saturated stem xylem |
| $k_{sax}$ [1] | $\text{m s}^{-1}$ | $1 \cdot 10^{-5}$ | Specific axial conductivity for the root system |
| $a_p$ [1] | $\text{Pa}^{-1}$ | $2 \cdot 10^{-6}$ | Xylem cavitation parameter |
| $b_p$ [1] | Pa | $-1.5 \cdot 10^{-6}$ | Xylem cavitation parameter |

[1] Definitions and equations using these parameters can be found in the Supplementary Material.

### 3.2.3 Results

The model predictions for sap-flux during the day compared well with observation during the entire measurement period (Fig.5a), reaching a $R^2$ value of 0.74. The model maintained a continuous water potential along roots and stem xylem (Fig. 5b). At midday, in the roots, water potential decreases almost linearly with elevation, while in the stem xylem, because of the

265 transpiration flux at the top of the tree, it is non linear. The change in the gradient at the soil surface is due to the sharp change in the axial hydraulic conductivity, since the xylem cross-sectional area index for the stem ($A_x/A_s$=8.6·$10^{-4}$) is different from that of the roots ($A_r/A_s$=1).

For the days shown in Fig.5b, during midday, when transpiration is usually peaking, water potential fluctuates between a minimum of -2.2 MPa at the tree top and -0.8 MPa at the bottom of the roots. This range of values is in agreement with the

270 results from the original studies and the published literature (Franks et al., 2007; Choat et al., 2012; Verma et al., 2014; Quijano and Kumar, 2015).
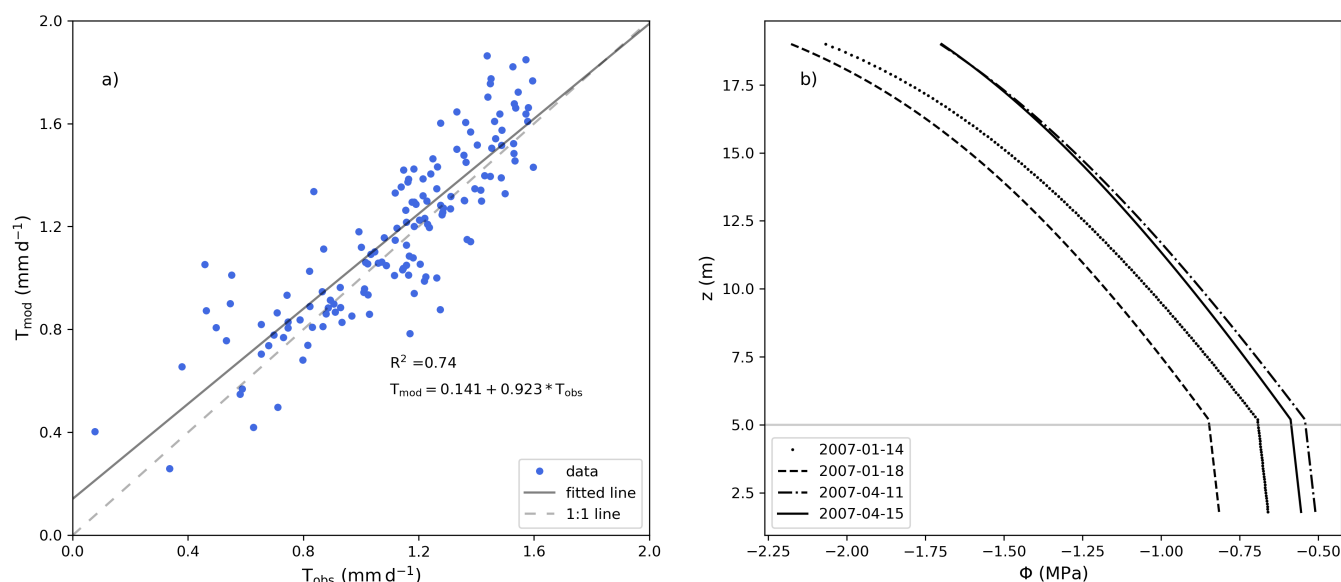


**Figure 5.** a) Comparison between measured ($T_{obs}$) and modelled ($T_{mod}$) daily sap flux rates excluding fluxes during the night. b) Root and stem water potential (MPa) as a function of elevation (z) at midday. The vertical position of 5 m (above z=0, which is defined as the bottom of the soil column) represents the interface between between the roots and the stem

A comparison of modelled and observed time series of transpiration rates for a week in January (summer) and April (autumn) is shown in Fig.6. The model is able to reproduce the temporal patterns of transpiration during the day, and does not show large fluxes at night, because of the simplified modelling of the stomatal conductance at night, as in Verma et al. (2014) (see

275 Supplementary Material).

SPAC-3Hpy was able to accurately represent the nonlinear interactions between the above- and below-ground components of the SPAC. From Fig 6, we can verify that root water uptake and transpiration are coupled, meaning that below-above ground interface is correctly represented by the model. Below-ground, shallow soil layers generated maximum rates of root water uptake (RWU) during most days, caused by greater root density and low water stress when water is readily available. During dryer days, with the decrease of soil moisture at the surface, considerable RWU was found in the deeper layers (approximately 20 - 30 cm from the soil surface). Root water uptake from deeper layers can be characterized as a hydraulic compensation path generated by rapid reductions in the top layers radial hydraulic conductivity, as it can be seen in Fig 6a, during the last 3 days in January.
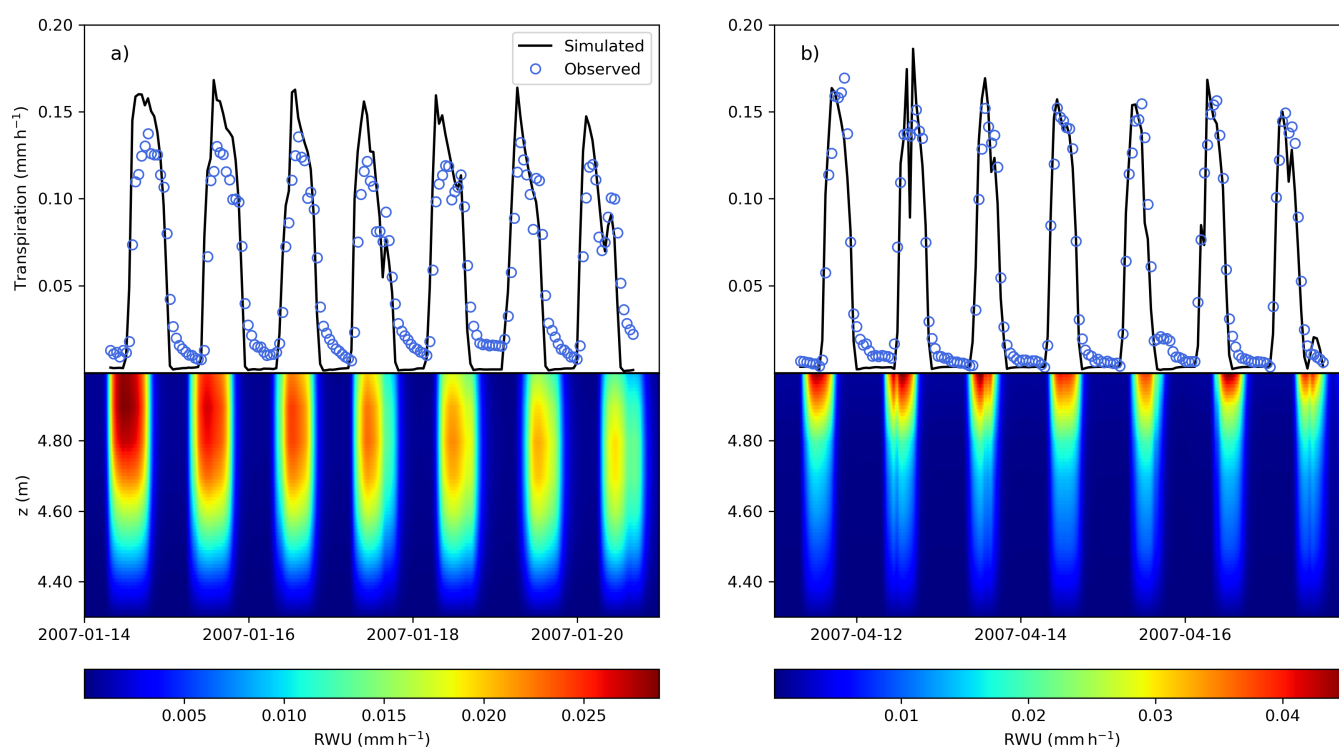


**Figure 6.** Comparison between modelled (black line) and observed (blue circles) transpiration rates and modelled root water uptake (colormap, $\mathrm{mm\,h^{-1}}$) during one-week periods in (a) January and in (b) April. The vertical position of 5 m (above z=0, which is defined as the bottom of the soil column) represents the interface between the roots and the above-ground stem xylem.

### 3.3 Modelling LAD and capacitance

SPAC-3Hpy is able to simulate the distribution of transpiration along the vertical axis, as well as a capacitance function for the roots and stem. In order to test this capability, we applied SPAC-3Hpy using the same parameters and setup as in section 3.2.2, but changed how the transpiration and capacitance are modelled in the case study. For this experiment, transpiration is

not a boundary condition at the tree top, but is distributed along the stem as in Eq. (3), with $S_x/A_s$ depending on the leaf area density (LAD). At the tree top, a no-flux condition is applied. An empirical LAD function described in Lalic and Mihailovic

290 (2004) was used, and a LAD profile suitable for *Eucalyptus* stands can be written as:

$$l(z) = l_{max} \left( \frac{h - z_m}{h - z} \right)^{n_0} \exp \left[ n_0 \left( 1 - \frac{h - z_m}{h - z} \right) \right], \tag{23}$$

where $h$ is the tree height (m), $l_{max}$ ($\mathrm{m^2\ m^{-3}}$) is the maximum value of leaf area density in a layer, $z_m$ (m) is the corresponding above-ground height of $l_{max}$, and $n_0$ (-) is an empirical parameter defined as

$$n_0 = \begin{cases} 6 & 0 \leq z < z_m, \\ 0.5 & z_m \leq z \leq h. \end{cases} \tag{24}$$

The value of $l_{max}$ can be calculated from the LAI imposing

295 $$LAI = \int_0^h l(z)dz. \tag{25}$$

Following Chuang et al. (2006) and Bohrer et al. (2005), the capacitance of the roots and stem xylem are

$$C_x(\Phi_x) = \frac{A_x}{A_s} \frac{\partial \theta_x}{\partial \Phi_x} = \frac{A_x p \theta_{sat,x}}{A_s \Phi_d} \left( \frac{\Phi_d - \Phi_x}{\Phi_d} \right)^{-(p+1)}, \tag{26}$$

$$C_r(\Phi_r) = \frac{A_r}{A_s} \frac{\partial \theta_r}{\partial \Phi_r} = \frac{A_r p \theta_{sat,r}}{A_s \Phi_d} \left( \frac{\Phi_d - \Phi_r}{\Phi_d} \right)^{-(p+1)}, \tag{27}$$

where $\Phi_d$ (Pa) and $p$ (-) are empirical coefficients for the hydraulic system, and $\theta_{sat,x}$ (-) and $\theta_{sat,r}$ (-) are the water content at

300 saturation for the stem and roots, respectively. The values of these parameters are shown in Table 4.

From Fig. 7, the vertical distribution of transpiration follows the shape of the LAD, with larger values of transpiration where the LAD is also large. Accordingly, $\Phi$ decreases along the tree height, in accordance with the no-flux boundary condition applied at the top of the tree.

## 4   Conclusions

305 The Soil-Plant-Atmosphere Continuum Tree Hydrodynamic model (SPAC-3Hpy) was introduced in this study. We tested SPAC-3Hpy against exact numerical solutions of the equations and observations of transpiration. The numerical scheme of the model was applied to two simplified exact non-steady state cases, reaching a maximum error of approximately 0.2% with respect to the exact solution at the tree top of a 6 m high tree, for a case in which transpiration is dependent on both time and elevation. For a steady-state scenario, considering a more complex formulation, the error approached 0.4% of the exact

310 solution at the tree top.
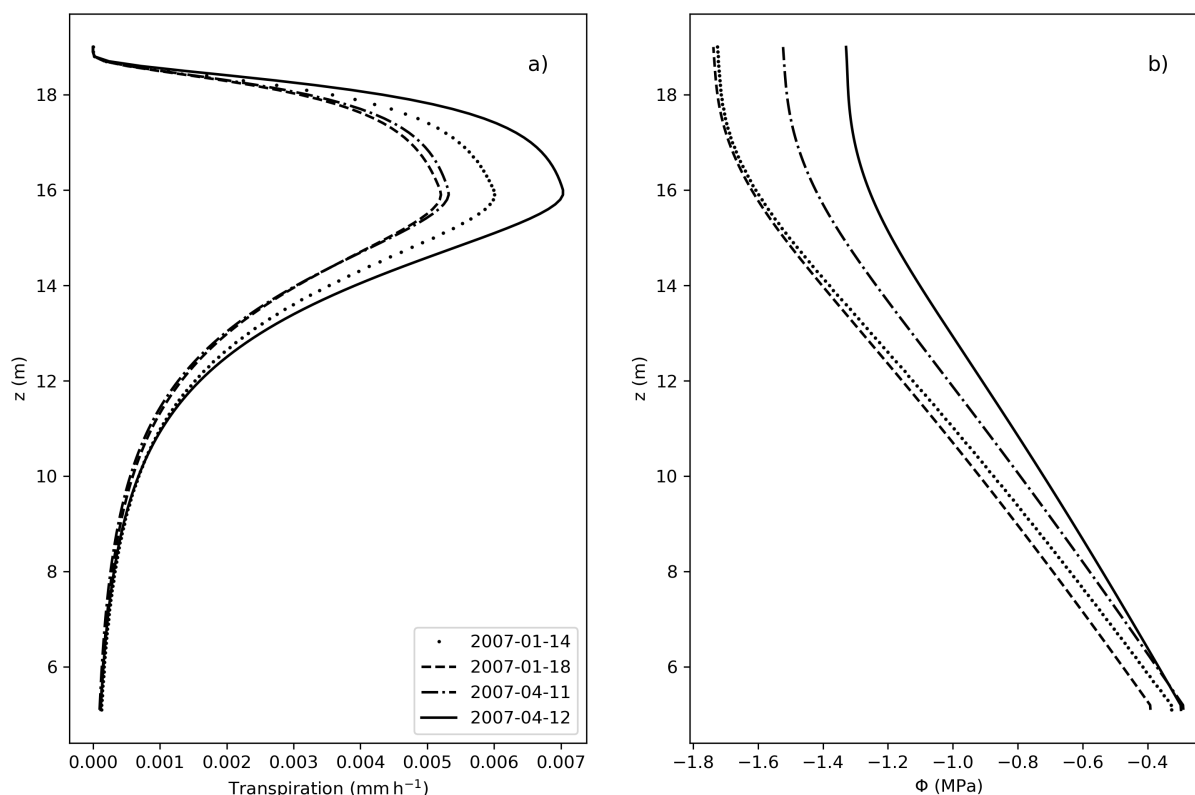
**Figure 7.** a) Transpiration fluxes ($\mathrm{mm\,h^{-1}}$) as a function of the elevation (z). b) Water potential (MPa) along z, considering z=0 at the bottom of the soil, and z=5 m equal the bottom of the stem xylem.

**Table 4.** List of parameters used in the application of the model considering a capacitance and a leaf area density function

| Parameters | Units | Value | Description |
|---|---|---|---|
| $l_{max}$ | $\mathrm{m^2 m^{-3}}$ | 0.4 | Maximum value of leaf area density |
| $z_m$ | m | 11 | Corresponding above-ground height of $l_{max}$ |
| $n_0$ | - | 6 or 0.5 | Empirical parameter (Eq. 24) |
| $\Phi_d$ | Pa | $5.74 \cdot 10^8$ | Empirical parameter for water pressure of dry xylem |
| $p$ | - | 20 | Empirical coefficient |
| $\theta_{sat,x}$ | - | 0.58 | Water content at saturation for the stem xylem |
| $\theta_{sat,r}$ | - | 0.58 | Water content at saturation for the root xylem |

Simulated transpiration rates from SPAC-3Hpy reached an $R^2$ of 0.74 in comparison to observed sapflow rates from a published case study. In addition, values of water potential were continuous along roots and stem xylem, showing that water flux in the soil, roots, and stem are correctly coupled along the entire tree structure. By using a hydrodynamic set of equations, SPAC-3Hpy

Geoscientific
Model Development
Discussions

EGU

Open Access

resolves the temporal and vertical dynamics of root water uptake, and stem and root water transport and storage. This allows
315 SPAC-3Hpy to simulate hydrodynamic phenomena such as root water compensation following reductions of soil moisture in the shallow soil layers.

By comparing the model predictions of transpiration and soil and xylem water storage, with different sets of parameters (describing the whole-tree hydraulic strategy of the trees), and different environmental forcing (describing realistic or hypothetical conditions and stress), SPAC-3Hpy will allow model-based studies of the consequences of hydraulic traits and strategies of dif-
320 ferent tree species for above- and below-ground water transport, with a range of stem and root xylem hydraulic characteristics.

*Code and data availability.* The development of SPAC-3Hpy model and graphs presented in this paper were conducted in Python 3. The exact version of SPAC-3Hpy used to produce the results can be found in the GitHub repository: https://github.com/mdef0001/SPAC-3Hpy.git

*Author contributions.* MS, AMM, and ED designed the study; MS, VRNP, and ED developed the model scripts; AMM, GB, DT, VRNP, and ED supervised the writing and results; MS and ED wrote the original draft. All authors gave comments and contributed to the final version
325 of the manuscript.

*Competing interests.* The authors declare that they have no conflict of interest

# References

Abramowitz, M. and Stegun, I. A.: Handbook of Mathematical Functions with Formulas, Graphs, and Mathematical Tables., JSTOR, https://doi.org/10.2307/2282672, 1964.

Allen, R., Pereira, L., Raes, D., and Smith, M.: Crop evapotranspiration - Guidelines for computing crop water requirements - FAO irrigation and drainage paper 56. Rome: FAO, 1998.

Amenu, G. G. and Kumar, P.: A model for hydraulic redistribution incorporating coupled soil-root moisture transport, Hydrology and Earth System Sciences Discussions, 4, 3719–3769, https://doi.org/10.5194/hessd-4-3719-2007, 2007.

Bartlett, M. S., Vico, G., and Porporato, A.: Coupled carbon and water fluxes in CAM photosynthesis: modeling quantification of water use efficiency and productivity, Plant and Soil, 383, 111–138, https://doi.org/10.1007/s11104-014-2064-2, 2014.

Bohrer, G., Mourad, H., Laursen, T. A., Drewry, D., Avissar, R., Poggi, D., Oren, R., and Katul, G. G.: Finite element tree crown hydrodynamics model (FETCH) using porous media flow within branching elements: A new representation of tree hydrodynamics, Water Resources Research, 41, https://doi.org/10.1029/2005wr004181, 2005.

Bohrer, G., Katul, G. G., Walko, R. L., and Avissar, R.: Exploring the effects of microscale structural heterogeneity of forest canopies using large-eddy simulations, Boundary-layer meteorology, 132, 351–382, 2009.

Bonan, G. B., Patton, E. G., Harman, I. N., Oleson, K. W., Finnigan, J. J., Lu, Y., and Burakowski, E. A.: Modeling canopy-induced turbulence in the Earth system: a unified parameterization of turbulent exchange within plant canopies and the roughness sublayer (CLM-ml v0), Geoscientific Model Development, 11, 1467–1496, https://doi.org/10.5194/gmd-11-1467-2018, 2018.

Broadbridge, P., Daly, E., and Goard, J.: Exact Solutions of the Richards Equation With Nonlinear Plant-Root Extraction, Water Resources Research, 53, 9679–9691, https://doi.org/10.1002/2017wr021097, 2017.

Celia, M. A., Bouloutas, E. T., and Zarba, R. L.: A general mass-conservative numerical solution for the unsaturated flow equation, Water Resources Research, 26, 1483–1496, https://doi.org/10.1029/wr026i007p01483, 1990.

Choat, B., Jansen, S., Brodribb, T. J., Cochard, H., Delzon, S., Bhaskar, R., Bucci, S. J., Feild, T. S., Gleason, S. M., Hacke, U. G., Jacobsen, A. L., Lens, F., Maherali, H., Martínez-Vilalta, J., Mayr, S., Mencuccini, M., Mitchell, P. J., Nardini, A., Pittermann, J., Pratt, R. B., Sperry, J. S., Westoby, M., Wright, I. J., and Zanne, A. E.: Global convergence in the vulnerability of forests to drought, Nature, 491, 752–755, https://doi.org/10.1038/nature11688, 2012.

Chuang, Y.-L., Oren, R., Bertozzi, A. L., Phillips, N., and Katul, G. G.: The porous media model for the hydraulic system of a conifer tree: Linking sap flux data to transpiration rate, Ecological Modelling, 191, 447–468, https://doi.org/10.1016/j.ecolmodel.2005.03.027, 2006.

Cowan, I. R.: Transport of Water in the Soil-Plant-Atmosphere System, Journal of Applied Ecology, 2, 221–239, https://doi.org/10.2307/2401706, http://www.jstor.org/stable/2401706, 1965.

Cruiziat, P., Cochard, H., and Améglio, T.: Hydraulic architecture of trees: main concepts and results, Annals of Forest Science, 59, 723–752, https://doi.org/10.1051/forest:2002060, 2002.

Daly, E., Porporato, A., and Rodriguez-Iturbe, I.: Coupled Dynamics of Photosynthesis, Transpiration, and Soil Water Balance. Part II: Stochastic Analysis and Ecohydrological Significance, Journal of Hydrometeorology, 5, 559–566, https://doi.org/10.1175/1525-7541(2004)005<0559:cdopta>2.0.co;2, 2004a.

Daly, E., Porporato, A., and Rodriguez-Iturbe, I.: Coupled dynamics of photosynthesis, transpiration, and soil water balance. Part I: Upscaling from hourly to daily level, Journal of Hydrometeorology, 5, 546–558, https://doi.org/10.1175/1525-7541(2004)005<0546:CDOPTA>2.0.CO;2, 2004b.

Drewry, D. T., Kumar, P., Long, S., Bernacchi, C., Liang, X.-Z., and Sivapalan, M.: Ecohydrological responses of dense canopies to environmental variability: 1. Interplay between vertical structure and photosynthetic pathway, Journal of Geophysical Research, 115, https://doi.org/10.1029/2010jg001340, 2010.

370    Fatichi, S., Pappas, C., and Ivanov, V. Y.: Modeling plant–water interactions: an ecohydrological overview from the cell to the global scale, WIREs Water, 3, 327–368, https://doi.org/10.1002/wat2.1125, 2016.

Franks, P. J., Drake, P. L., and Froend, R. H.: Anisohydric but isohydrodynamic: seasonally constant plant water potential gradient explained by a stomatal control mechanism incorporating variable plant hydraulic conductance, Plant, Cell and Environment, 30, 19–30, https://doi.org/10.1111/j.1365-3040.2006.01600.x, 2007.

375    Fruh, T. and Kurth, W.: The Hydraulic System of Trees: Theoretical Framework and Numerical Simulation, Journal of Theoretical Biology, 201, 251–270, https://doi.org/10.1006/jtbi.1999.1028, 1999.

Gardner, W. R.: Dynamic aspects of water availability to plants, Soil Science, 89, 63–73, https://doi.org/10.1097/00010694-196002000-00001, 1960.

Hartzell, S., Bartlett, M. S., and Porporato, A.: Unified representation of the C3, C4, and CAM photosynthetic pathways with the Photo3

380    model, Ecological Modelling, 384, 173–187, https://doi.org/10.1016/j.ecolmodel.2018.06.012, 2018.

Herkelrath, W. N., Miller, E. E., and Gardner, W. R.: Water Uptake By Plants: II. The Root Contact Model, Soil Science Society of America Journal, 41, 1039–1043, https://doi.org/10.2136/sssaj1977.03615995004100060004x, 1977.

Huang, C.-W., Domec, J.-C., Ward, E. J., Duman, T., Manoli, G., Parolari, A. J., and Katul, G. G.: The effect of plant water storage on water fluxes within the coupled soil-plant system, New Phytologist, 213, 1093–1106, https://doi.org/10.1111/nph.14273, 2017.

385    Janott, M., Gayler, S., Gessler, A., Javaux, M., Klier, C., and Priesack, E.: A one-dimensional model of water flow in soil-plant systems based on plant architecture, Plant and Soil, 341, 233–256, https://doi.org/10.1007/s11104-010-0639-0, 2011.

Jarvis, N. J.: The interpretation of the variations in leaf water potential and stomatal conductance found in canopies in the field, Philosophical Transactions of the Royal Society of London. B, Biological Sciences, 273, 593–610, https://doi.org/10.1098/rstb.1976.0035, 1976.

Jones, H. G.: Plants and Microclimate, Cambridge University Press, https://doi.org/10.1017/cbo9780511845727, 2009.

390    Katul, G. G., Oren, R., Manzoni, S., Higgins, C., and Parlange, M. B.: Evapotranspiration: A process driving mass transport and energy exchange in the soil-plant-atmosphere-climate system, Reviews of Geophysics, 50, https://doi.org/10.1029/2011rg000366, 2012.

Kumagai, T.: Modeling water transportation and storage in sapwood — model development and validation, Agricultural and Forest Meteorology, 109, 105–115, https://doi.org/10.1016/s0168-1923(01)00261-1, 2001.

Lalic, B. and Mihailovic, D. T.: An Empirical Relation Describing Leaf-Area Density inside the Forest for Environmental Modeling, Journal

395    of Applied Meteorology, 43, 641–645, https://doi.org/10.1175/1520-0450(2004)043<0641:aerdld>2.0.co;2, 2004.

Li, L., Yang, Z.-L., Matheny, A. M., Zheng, H., Swenson, S. C., Lawrence, D. M., Barlage, M., Yan, B., McDowell, N. G., and Leung, L. R.: Representation of Plant Hydraulics in the Noah-MP Land Surface Model: Model Development and Multiscale Evaluation, Journal of Advances in Modeling Earth Systems, 13, 2021.

Manoli, G., Bonetti, S., Domec, J.-C., Putti, M., Katul, G., and Marani, M.: Tree root systems competing for soil moisture in a 3D soil–plant

400    model, Advances in Water Resources, 66, 32–42, https://doi.org/10.1016/j.advwatres.2014.01.006, 2014.

Manzoni, S., Vico, G., Porporato, A., and Katul, G.: Biological constraints on water transport in the soil–plant–atmosphere system, Advances in Water Resources, 51, 292–304, 2013.

Matheny, A. M., Mirfenderesgi, G., and Bohrer, G.: Trait-based representation of hydrological functional properties of plants in weather and ecosystem models, Plant Diversity, 39, 1–12, https://doi.org/10.1016/j.pld.2016.10.001, 2017.

405    Mencuccini, M., Manzoni, S., and Christoffersen, B.: Modelling water fluxes in plants: from tissues to biosphere, New Phytologist, 222, 1207–1222, https://doi.org/10.1111/nph.15681, 2019.

Mendel, M., Hergarten, S., and Neugebauer, H. J.: On a better understanding of hydraulic lift: A numerical study, Water Resources Research, 38, 1–1–1–10, https://doi.org/10.1029/2001wr000911, 2002.

Mirfenderesgi, G., Bohrer, G., Matheny, A. M., Fatichi, S., de Moraes Frasson, R. P., and Schäfer, K. V. R.: Tree level hydrodynamic
410    approach for resolving aboveground water storage and stomatal conductance and modeling the effects of tree hydraulic strategy, Journal of Geophysical Research: Biogeosciences, 121, 1792–1813, https://doi.org/10.1002/2016jg003467, 2016.

Mirfenderesgi, G., Matheny, A. M., and Bohrer, G.: Hydrodynamic trait coordination and cost-benefit trade-offs throughout the isohydric-anisohydric continuum in trees, Ecohydrology, 12, e2041, https://doi.org/10.1002/eco.2041, 2018.

Nobel, P. S.: Chapter 9 - Plants and Fluxes, pp. 438–505, Academic Press, San Diego, https://doi.org/https://doi.org/10.1016/B978-0-12-
415    374143-1.00009-0, 2009.

Polyanin, A. D.: Handbook of Linear Partial Differential Equations for Engineers and Scientists, Chapman and Hall/CRC, https://doi.org/10.1201/9781420035322, 2001.

Quijano, J. C. and Kumar, P.: Numerical simulations of hydraulic redistribution across climates: The role of the root hydraulic conductivities, Water Resources Research, 51, 8529–8550, 2015.

420    Shaw, R. H. and Schumann, U.: Large-eddy simulation of turbulent flow above and within a forest, Boundary-Layer Meteorology, 61, 47–64, https://doi.org/10.1007/bf02033994, 1992.

Somma, F., Hopmans, J. W., and Clausnitzer, V.: Transient three-dimensional modeling of soil water and solute transport with simultaneous root growth, root water and nutrient uptake, Plant and Soil, 202, 281–293, https://doi.org/10.1023/A:1004378602378, 1998.

Steudle, E.: The Cohesion-Tension Mechanism and the Acquisition of Water by Plant Roots, Annual Review of Plant Physiology and Plant
425    Molecular Biology, 52, 847–875, https://doi.org/10.1146/annurev.arplant.52.1.847, 2001.

Teodosio, B., Pauwels, V. R. N., Loheide, S. P., and Daly, E.: Relationship between root water uptake and soil respiration: A modeling perspective, Journal of Geophysical Research: Biogeosciences, 122, 1954–1968, https://doi.org/10.1002/2017jg003831, 2017.

van den Honert, T. H.: Water transport in plants as a catenary process, Discussions of the Faraday Society, 3, 146, https://doi.org/10.1039/df9480300146, 1948.

430    van Genuchten, M. T.: A Closed-form Equation for Predicting the Hydraulic Conductivity of Unsaturated Soils, Soil Science Society of America Journal, 44, 892–898, https://doi.org/10.2136/sssaj1980.03615995004400050002x, 1980.

Verma, P., Loheide, S. P., Eamus, D., and Daly, E.: Root water compensation sustains transpiration rates in an Australian woodland, Advances in Water Resources, 74, 91–101, https://doi.org/10.1016/j.advwatres.2014.08.013, 2014.

Yunusa, I. A. M., Zolfaghar, S., Zeppel, M. J. B., Li, Z., Palmer, A. R., and Eamus, D.: Fine Root Biomass and Its Relationship to Evapo-
435    transpiration in Woody and Grassy Vegetation Covers for Ecological Restoration of Waste Storage and Mining Landscapes, Ecosystems, 15, 113–127, https://doi.org/10.1007/s10021-011-9496-9, 2012.

Zeppel, M., Macinnis-Ng, C., Palmer, A., Taylor, D., Whitley, R., Fuentes, S., Yunusa, I., Williams, M., and Eamus, D.: An analysis of the sensitivity of sap flux to soil and plant variables assessed for an Australian woodland using a soil - plant - atmosphere model, Functional Plant Biology, 35, 509, https://doi.org/10.1071/fp08114, 2008.